New Journal of Physics
The open-access journal for physics

Spin photocurrents in (110)-grown quantum well structures

H Diehl[1], V A Shalygin[1,2], V V Bel'kov[1,3], Ch Hoffmann[1], S N Danilov[1], T Herrle[1], S A Tarasenko[3], D Schuh[1], Ch Gerl[1], W Wegscheider[1], W Prettl[1] and S D Ganichev[1,4]

[1] Fakultät Physik, University of Regensburg, 93040 Regensburg, Germany
[2] St. Petersburg State Polytechnic University, 195251 St. Petersburg, Russia
[3] A F Ioffe Physico-Technical Institute, Russian Academy of Sciences, 194021 St. Petersburg, Russia
E-mail: sergey.ganichev@physik.uni-regensburg.de

New Journal of Physics **9** (2007) 349
Received 8 May 2007
Published 28 September 2007
Online at http://www.njp.org/
doi:10.1088/1367-2630/9/9/349

Abstract. The circular photogalvanic effect and the circular photon drag effect are observed and investigated in detail in (110)-grown quantum well structures. The experimental data are well described by phenomenological theory and microscopic models of both effects are developed being in agreement with experimental data.

Contents

[4] Author to whom any correspondence should be addressed.

PII: S1367-2630(07)50100-X

1. Introduction

The spin transport in semiconductor nanostructures is one of the key problems of semiconductor spintronics. Spin–orbit coupling provides a versatile tool to generate and to manipulate the spin degree of freedom in semiconductors. In low-dimensional structures based on III–V compound materials spin–orbit coupling removes the spin degeneracy of the energy bands in **k**-space, where **k** is the electron wavevector. This lifting of spin degeneracy is crucial for the field of spintronics. Indeed, spin-splitting of the subbands allows electric field control of spin polarization and spin relaxation, determines the spin relaxation rate by the D'yakonov–Perel' mechanism, and makes possible spin manipulation by an external electric field. An important parameter for semiconductor spintronics is the spin relaxation time: it must be sufficiently long for processing of information encoded as spin polarization. It was shown that in (110)-grown GaAs/AlGaAs quantum wells (QWs) the spin relaxation time is considerably longer compared to that in (001)-oriented QWs. It can reach several nanoseconds even at room temperature and may be controlled by an electrical field applied in the growth direction [1]–[4]. The reason for this extraordinarily long spin lifetime is that in symmetric (110)-grown QWs the in-plane spin splitting is absent because in this symmetry on the one hand there is no Rashba spin–orbit splitting and on the other hand the Dresselhaus spin splitting is present only for spins pointing normal to the plane of the QW. As a result, for spins oriented normal to the plane of the QW, the main spin relaxation mechanism which is caused by spin splitting (D'yakonov–Perel' mechanism) is suppressed. The observed increase of spin lifetimes has attracted a great deal of attention to spin dependent phenomena in (110)-oriented structures. An effective access to these phenomena in low-dimensional structures is provided by spin photocurrents like the circular photogalvanic effect (CPGE) [5]–[7] and the spin-galvanic effect (SGE) [8], allowing investigation of spin relaxation times, spin splitting of the band structure, symmetry properties, etc (for a review see [9, 10]). So far spin photocurrents were mostly studied in (001)- and (113)-grown heterostructures.

Here, we report on the observation and study of spin photocurrents in (110)-grown GaAs/AlGaAs QW structures. It is demonstrated that an optical excitation of QW structures with circularly polarized radiation leads to a current whose direction and magnitude depends on the degree of circular polarization of the incident light. The investigated effects comprise the CPGE and the circular photon drag effect predicted a long time ago [11, 12] but so far not observed. The CPGE can be considered as a transfer of the photon angular momentum to a directed motion of a free charge carriers. The circular photon drag effect is caused by transfer of both angular and linear momenta of photons to free carriers. The photon drag effect solely due to the transfer of linear momentum from photons, the so-called linear photon drag effect, is a well-known phenomenon (see e.g. [9], [13]–[16]). It is present in both noncentrosymmetric and in centrosymmetric semiconductor systems and the inversion of the light helicity does not affect the sign and magnitude of the linear photon drag current. The circular photon drag effect reported here, in contrast, represents a photon drag current which reverses its direction by inversion of the light helicity from left-handed to right-handed and vice versa and is allowed in gyrotropic media only. A significant part of this work has most recently been published in [17]. The measurements of photocurrents are carried out under excitation of samples with infrared radiation at normal and oblique incidence. Infrared radiation is used to excite *inter*-subband transitions between the lowest and the first excited subbands of the investigated QWs. The experimental data are well described by analytical expressions derived

from a phenomenological theory and fit well to the microscopic picture of CPGE [9, 10]. A microscopic model of the circular photon drag effect is also developed demonstrating that the generated current has spin dependent origin.

2. Experimental technique

For optical excitation mid-infrared (MIR) and terahertz (THz) laser radiation is used. Depending on the photon energy and the QW band structure the MIR and THz radiation induce direct optical transitions between size quantized subbands or, at longer wavelength, indirect optical transitions (Drude absorption) in the lowest subband. The source of MIR radiation is a Q-switched CO_2-laser with operating spectral range (9.2–10.8 μm) corresponding to *inter*-subband transitions between the lowest and the first excited subbands of the investigated QWs. The Q-switched CO_2-laser operating at a frequency of 300 Hz provides radiation pulses with a pulse duration of about 300 ns. High power pulsed THz radiation is obtained by applying a molecular laser optically pumped by a transversely excited atmospheric pressure carbon dioxide (TEA-CO_2) [9]. Several wavelengths between 77 and 496 μm have been selected using NH_3, D_2O and CH_3F as active media. Typically these lasers emit linearly polarized radiation. The polarization is modified from linear to circular using a Fresnel rhomb and $\lambda/4$ plates for MIR and FIR radiation, respectively. The helicity $P_{\rm circ}$ of the incident light is varied from -1 (left-handed circular, σ_-) to +1 (right-handed circular, σ_+) according to $P_{\rm circ} = \sin 2\varphi$. In the present experimental arrangement, the phase angle φ corresponds to the angle between the initial plane of polarization and the optical axis of the $\lambda/4$ plate or the polarization plane of the Fresnel rhomb.

Measurements of photocurrents are carried out under excitation of the samples with infrared or terahertz radiation at normal and oblique incidence. The geometry of the experiment is sketched in the insets in figures 1 and 4. The photocurrent is measured in unbiased structures via the voltage drop across a 50 Ω load resistor. The experiments are carried out at room temperature on asymmetrical (110)-oriented GaAs/$Al_{0.34}Ga_{0.66}As$ molecular beam epitaxy grown heterostructures containing 100 QWs of 8.2 nm width separated by 40 nm barriers. Two n-type structures with electron concentration n_s about 7×10^{11} cm^{-2} per QW and various doping profiles are investigated. The sample A contains Si-doped layers of 10 nm width in each barrier shifted from the barrier center by the distance of 10 nm. In sample B, the doped layer of the same width is placed in the center of each barrier. Samples have sizes about 5×5 mm^2. The sample edges are oriented along $x \parallel [1\bar{1}0]$ and $y \parallel [00\bar{1}]$ in the QW plane, the z-axis points parallel to the structure growth direction. To measure electrical currents ohmic contacts are prepared in the center of each sample edge.

3. Experimental results and discussion

3.1. Normal incidence

Irradiating the samples at normal incidence results in a photocurrent j_x whose temporal structure reproduces that of the laser pulse as shown in figure 1.

The data are well described by the sum of two terms: one of them is proportional to $\sin 2\varphi$ and the other $\propto \sin 4\varphi$. This behavior, also obtained at THz excitation, can be understood from

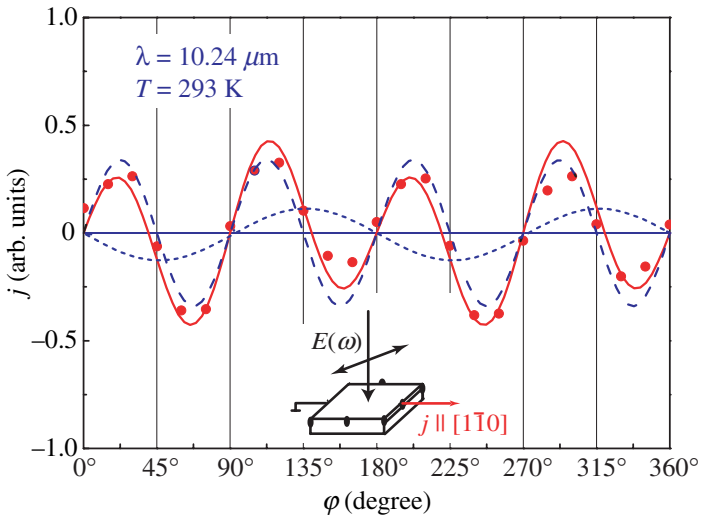

Figure 1. Photogalvanic current in (110)-grown GaAs QWs (sample B) as a function of the phase angle φ. The results were obtained at $\lambda = 10.6\,\mu$m under normal incidence of irradiation at room temperature. The full line corresponding to the sum of CPGE and linear photogalvanic effect (LPGE) is fitted by angle dependences of the photocurrent after $j_x = j_1 \sin 2\varphi + j_2 \sin 4\varphi$ (see (3)), where j_1 and j_2 are the ordinate scaling parameters. Dotted and broken lines show $j_x = j_1 \sin 2\varphi$ and $j_x = j_2 \sin 4\varphi$, respectively.

the phenomenological theory which yields

$$j_\lambda = \chi_{\lambda\mu\nu} \left(E_\mu(\omega) E^*_\nu(\omega) + E^*_\mu(\omega) E_\nu(\omega) \right) /2 + \mathrm{i}\gamma_{\lambda\kappa} \left(\mathbf{E} \times \mathbf{E}^* \right)_\kappa , \tag{1}$$

where $\chi_{\lambda\mu\nu}$ is a third rank tensor and $\gamma_{\lambda\kappa}$ is a second-rank pseudo-tensor.

The second term on the right-hand side of (1) can be expressed using $\mathrm{i}(\mathbf{E} \times \mathbf{E}*)_\kappa = \hat{e}_\kappa P_{\mathrm{circ}} E_0^2$ with E_0 being the electric field amplitude $|\mathbf{E}|$. Because of the factor P_{circ}, indicating the degree of circular polarization, this term is identified with the CPGE [5] and optical orientation induced SGE [8], while the first term of (1) contributes also for linearly polarized light and hence represents the LPGE [9, 10, 18, 19]. Both effects exist only in systems without a center of inversion. For the case of C_s symmetry relevant to the samples investigated here and at normal incidence (1) reduces to the form

$$j_x = \chi_{xxy} \left(e_x e^*_y + e_y e^*_x \right) E_0^2 + \gamma_{xz} E_0^2 P_{\mathrm{c}}, \tag{2}$$

and gives an analytical dependence of the current on the phase angle φ

$$j_x = \chi_{xxy} E_0^2 \sin 4\varphi + \gamma_{xz} E_0^2 \sin 2\varphi. \tag{3}$$

Therefore the observed interplay of two terms can be attributed to current contributions caused by circular ($j_x \propto \sin 2\varphi$) and linear ($j_x \propto \sin 4\varphi$) photogalvanic effects. As it is seen from figure 1 both contributions are of the same order of magnitude which makes possible their experimental separation. In the present work, we examine only helicity dependent photocurrents, i.e. currents which reverse their sign upon switching the radiation helicity. In order to extract such a current contribution, $J_x^{\mathrm{circ}} \propto P_{\mathrm{circ}}$, from the measured total current we determined the response to σ_+ and σ_- radiation and evaluated the data after

$$J_x^{\mathrm{circ}} = \left[J_x(\sigma_+) - J_x(\sigma_-) \right] /2 . \tag{4}$$

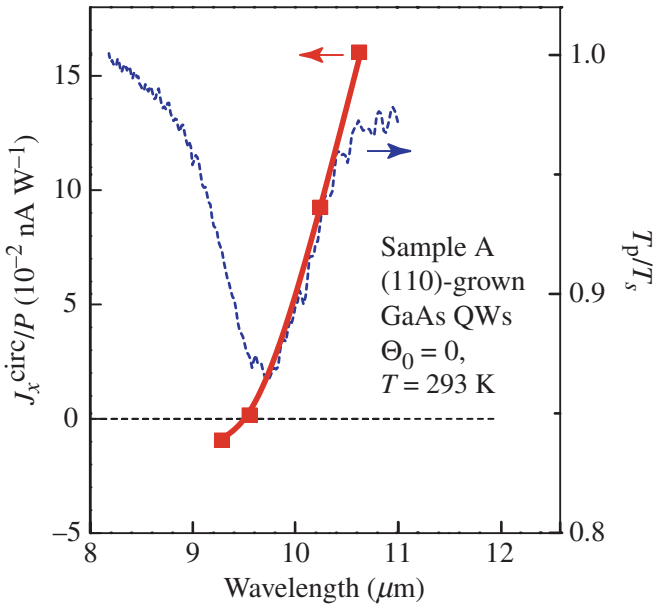

Figure 2. Spectrum of helicity dependent photocurrent J_x^{circ} normalized to the laser power P measured in sample A illuminated by infrared laser radiation under normal incidence (squares) and spectrum of optical transmission ratio $T_\mathrm{p}/T_\mathrm{s}$ (dashed line) for light of p- and s-polarization, respectively. The solid line is a guide to the eye. The transmission spectrum is measured under oblique incidence at $\Theta_0 = 60^\circ$.

Investigating the spectral behavior of the photocurrent excited by the MIR radiation, we observe that the current for both left- and right-handed circular polarizations changes sign at a frequency $\omega = \omega_{\mathrm{inv}}$. This inversion frequency ω_{inv} coincides with the frequency of the absorption peak.

In figure 2, the photocurrent J_x^{circ} as a function of photon energy is plotted together with the absorption spectrum. The data are presented for sample A measured at room temperature. The fact that the photocurrent changes sign by tuning the wavelength indicates that it is mainly caused by the CPGE outweighing the SGE [20].

The physical origin of the CPGE illustrating the spectral sign inversion of the current at the center of the absorption line is sketched in figure 3 after [21]. In zinc-blende QW structures the degeneracy in **k**-space is lifted due to the spin–orbit coupling. In asymmetrical (110)-oriented samples the $\sigma_z k_x$ contribution to the Hamiltonian, responsible for the effect under normal incidence, splits the electron spectrum into spin sub-levels with the spin components $s_z = \pm 1/2$ along the growth direction z (σ_z is a Pauli matrix). As a result of optical selection rules, normally incident circularly polarized radiation, e.g. σ_-, induces direct optical transitions from the subband $e1$ with the spin $s_z = +1/2$ to the subband $e2$ with $s_z = -1/2$. Monochromatic radiation with a certain photon energy, say $h\omega_1 > \varepsilon_{21}$, induces the transitions only at a fixed wavevector k_x^- where the photon energy matches the transition energy as indicated by the vertical arrow in figure 3(a). Thus, the intersubband excitation results in an imbalance of the momentum distribution between positive and negative k_x in both subbands yielding an electric current. As in our QWs the energy separation between the subbands ε_{21} is larger than the

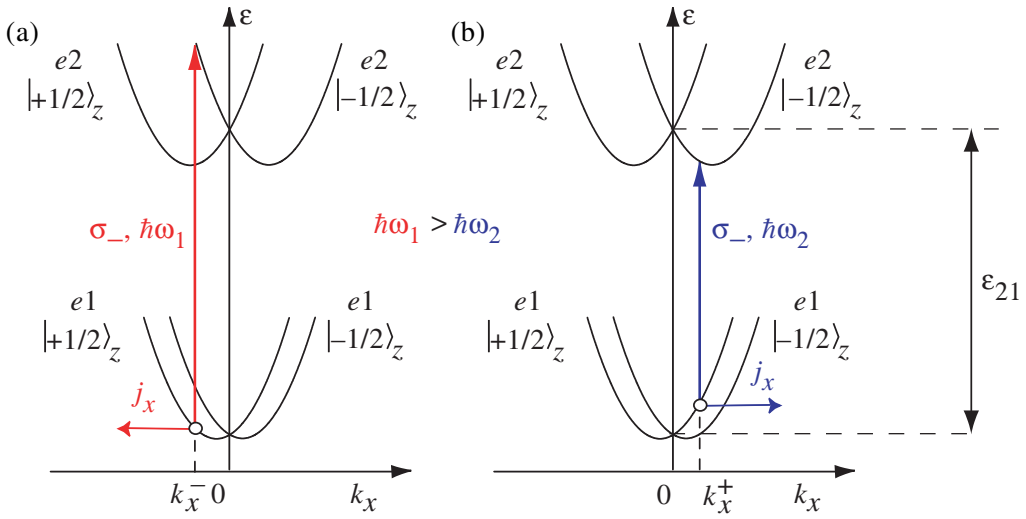

Figure 3. Microscopic picture describing the origin of the inversion of the photocurrent in C_s point group samples. The essential ingredient is the splitting of the conduction band due to k-linear terms. Right-handed circularly polarized radiation, σ_-, induces direct spin-flip transitions (vertical arrows) from $e1$ subband with $s_z = +1/2$ to $e2$ subband with $s_z = -1/2$. As a result an unbalanced occupation of the k_x states occurs yielding a spin polarized photocurrent. (a) For transitions with k_x^- left of the minimum of $e1$ ($s_z = +1/2$) subband the current indicated by j_x is negative. (b) At smaller $h\omega$ the transition occurs at k_x^+, now right of the subband minimum, and the current reverses its sign.

energy of longitudinal optical phonons ($\varepsilon_{21} \approx 100$ meV, $\hbar\Omega_{\mathrm{LO}} = 35$ meV), the nonequilibrium distribution of electrons in the subband $e2$ relaxes rapidly due to the emission of phonons. In this way, the contribution of the subband $e2$ to the electric current vanishes. Therefore, the magnitude Y and the direction of the current j_x, shown in figure 3(a) by the horizontal arrow, is determined by the group velocity and the momentum relaxation time τ_{e1} of the photogenerated 'holes' in the subband $e1$. Obviously, the whole picture mirrors and the current direction reverses by switching the circular polarization from left- to right-handed. Spectral inversion of the photocurrent at fixed helicity also follows from this model picture. Indeed, as is shown in figure 3(b), decreasing the photon frequency to $\hbar\omega_2$ shifts the transitions toward positive k_x and the direction of the current reverses (horizontal arrow). The inversion of the current direction takes place at the photon energy corresponding to the optical transitions from the spin subband minima. This mechanism is based on the Dresselhaus spin splitting due to $\sigma_z k_x$ terms and predicts, in accordance with the phenomenological theory, that the current reaches a maximum at normal incidence and becomes smaller under oblique incidence keeping the same direction.

3.2. Oblique incidence

Now we consider the dependence of the $j_x^{\mathrm{circ}} = j_x(\sigma_+) - j_x(\sigma_-)$ on the angle of incidence Θ for excitation in the xz-plane. For C_s-symmetry the phenomenological theory yields

$$j_x^{\mathrm{circ}} = \gamma_{xz}\, t_p t_s \frac{q_z}{q} E_0^2. \tag{5}$$

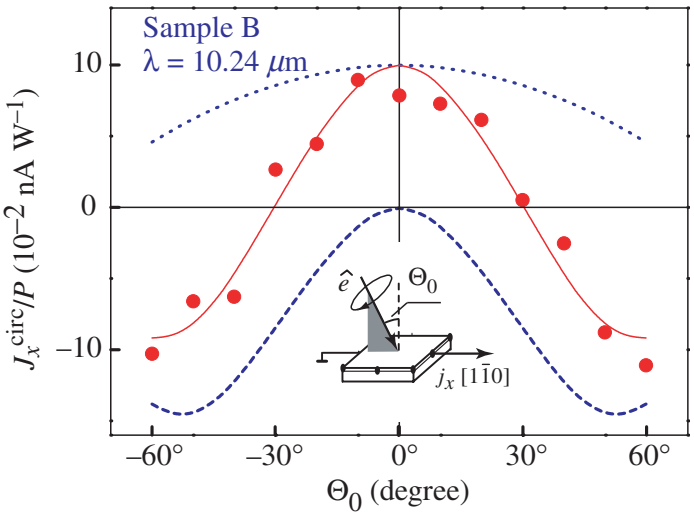

Figure 4. Normalized helicity dependent photocurrent J_x^{circ}/P obtained for sample B as a function of the angle of incidence Θ_0. The dotted, dashed and solid curves are fits after (8) and represent the term in square brackets, the last term on the right-hand side of (8), and the sum of both terms, respectively. The inset shows the geometry of the experiment.

where t_p and t_s are the transmission coefficients for the p and s polarization components of the light electric field, q is the light wavevector inside the medium. The dependence of the photocurrent on the angle of incidence Θ_0 is given by $q_z/q = \cos\Theta$ and by Fresnel's formulas for t_p and t_s,

$$t_p t_s = \frac{4\cos^2\Theta_0}{(\cos\Theta_0 + n_\omega\cos\Theta)(n_\omega\cos\Theta_0 + \cos\Theta)}, \tag{6}$$

where Θ is the angle of refraction defined by $\sin\Theta = \sin\Theta_0/n_\omega$, and n_ω is the refractive index of the medium.

In the whole THz range, where the photocurrent is caused by Drude absorption, we found that the dependence of the current J_x^{circ} on the angle of incidence is well described by (5) and (6). However, in the infrared range a significant discrepancy to these equations is observed. In contrast to the sign conserving behavior of the photocurrent given by $t_p t_s \cos\Theta$, the signal in the samples changes its sign twice (see figure 4)[5]. For the sample B the inversion takes place at $\Theta_0 \approx \pm 30^\circ$. This inversion of the current direction as a function of the angle of incidence cannot be explained in the framework of the conventional theory of the CPGE or the optically excited spin-galvanic effect. These theories ignore the linear momentum transfer from photons to free carriers. Taking into account the linear momentum of the photon, neglected previously in (1) and (5), we obtain an additional contribution to the current excited by circularly polarized

[5] We note that at oblique incidence a substantial helicity independent contribution to the total current is found. This contribution is due to the linear photogalvanic effect [15, 16] and the linear photon drag effect [14, 15], which are out of the scope of this paper. Nevertheless, the helicity dependent contribution J_x^{circ} is large enough compared to this background current and is easily measurable.

light. Then, the total helicity dependent photocurrent in structures of C_s symmetry is given by

$$j_x = t_p t_s \left\{ \left[(\gamma_{xz} + q_z T_{xzz}) \frac{q_z}{q} \right] + q_x T_{xxx} \frac{q_x}{q} \right\} E_0^2 P_c \,, \tag{7}$$

where $\mathbf{T}$ is the third rank tensor which describes the circular photon drag effect. Following (7) one obtains the angular dependence of the photocurrent

$$j_x = t_p t_s \left\{ \left[(\gamma_{xz} + q T_{xzz} \cos\Theta) \cos\Theta \right] + q T_{xxx} \sin^2\Theta \right\} E_0^2 P_c. \tag{8}$$

Equation (8) shows that the circular photon drag effect given by terms containing the linear photon momentum $\mathbf{q}$ can be observed, in principle, at both normal ($\Theta = 0$) and oblique incidence. However, the distinction between contributions of the CPGE and of the circular photon drag effect for $\Theta = 0$ is not an easy task. It may be done keeping in mind that the replacement $P_c \to -P_c$ and $q_z \to -q_z$ in (7) conserves the first term in the square brackets on the right-hand side of (7) while changing the sign of the second term. Experimentally it can be realized by putting a mirror behind the sample and comparing the current magnitudes with and without the mirror. However, such a method requires very high accuracy of adjustment.

Much more reliable access to the circular photon drag effect is provided by studying the angular dependence of the photocurrent. Indeed, the terms in square brackets in (8) have a maximum at normal incidence and their contribution to the current decreases with increasing angle of incidence. At the same time the circular photon drag effect given by the last term in (8) vanishes at normal incidence and increases with $|\Theta_0|$. This interplay of the current contributions may result in the observed two-fold sign inversion of the total current by the variation of Θ_0 from $-\pi/2$ to $\pi/2$, if the circular photon drag and the CPGE photocurrents flow in opposite directions. The fits of (8) to the experimental data for structure B is shown in figure 4. The plotted curves represent the terms in square brackets (dotted curves), the last term on the right-hand side of (8) (dashed curves), and the sum of both terms (solid curves). To fit the data, we use an ordinate scaling parameter for the dotted curve to obtain agreement at normal incidence, where the last term on the right-hand side of (8) vanishes. Then, the dashed curve is scaled to fit the data in the whole range of the angle of incidence Θ_0. It is seen that the phenomenological equation (8) describes well the experimental angular dependence of the photocurrent. The contribution to the circular photon drag effect given by the component T_{xxx} reaches its maximum at $\Theta_0 \approx \pm 50^\circ$.

4. Microscopic model of circular photon drag effect

Now we discuss the microscopic picture of the observed circular photon drag effect given by the last term on the right-hand side of (7). The tensor $\mathbf{T}$ is not invariant under time inversion. Therefore, dissipative processes should be involved in the microscopic model of the effect. The proposed model includes three stages.

The first stage is a helicity and photon wavevector dependent photoexcitation. The intersubband absorption of circularly polarized radiation is a spin dependent process. While at normal incidence the absorption of circularly polarized light is due to spin-flip processes (see figure 3), under oblique excitation due to selection rules the absorption is dominated by spin conserving transitions [22]. However, the rates of these spin conserving transitions are different for electrons with the spin oriented parallel and antiparallel to the in-plane direction of light propagation (x in figure 5(a)). In figure 5(b), the dominating optical transitions are

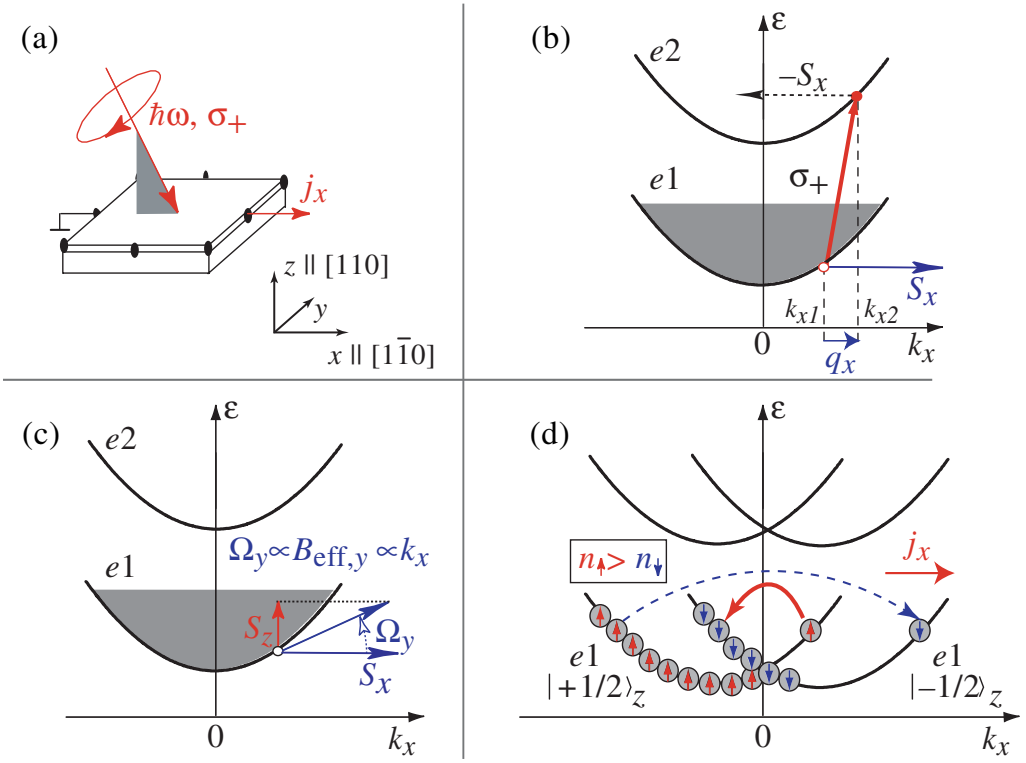

Figure 5. Sketch of the geometry of the experiment (a) and the three sequential stages of the microscopic model of the circular photon drag effect: (b) helicity and photon wavevector dependent photoexcitation, (c) spin rotation in an effective magnetic field caused by spin–orbit coupling, and (d) asymmetrical spin relaxation resulting in an electric current flow due to the SGE.

sketched by an inclined arrow to take into account the linear momentum of the photon involved. As a result of the linear momentum transfer the optical transitions occur at a distinct initial electron wavevector determined by energy and momentum conservation. The angular momenta of photons yield a spin polarization S_x at k_{x1} and $-S_x$ at k_{x2} in the subbands $e1$ and $e2$, respectively. These spin polarizations are indicated in figure 5(b) by solid and dashed horizontal arrows. While optical excitation results in a spin polarization at well determined wavevectors, k_{x1} in the subband $e1$ and k_{x2} in $e2$, the electrons in the upper subband have sufficient energy to emit optical phonons and rapidly relax due to this process. Thus, the spin polarization S_x in the lower subband only is connected with electrons with the well defined momentum (k_{x1} in figure 5(b)).

The second stage is spin precession in an effective magnetic field caused by the Rashba or the Dresselhaus spin–orbit coupling. The orientation and the strength of this effective magnetic field is determined by the direction and the magnitude of the electron wave vector. As our optical excitation results in the spin polarization S_x of electrons with the certain wavevector k_{x1}, the effective magnetic field linked to this wavevector acts on the electron spin. The spins of the electrons, directed just after photoexcitation along the x-axis, precess in the effective magnetic field which has both $\Omega_z \propto k_x$ and $\Omega_y \propto k_x$ components. As a consequence of the precession the spin components S_y and S_z appear, see figure 5(c) for component S_z. Under steady-state

excitation the generation rates of the spin components S_y and S_z are determined by the average angle of spin rotation in the effective magnetic field.

In the third stage, the nonequilibrium spin polarization S_z obtained in the first two stages of the proposed model description drives an electric current. This is due to the SGE caused by asymmetric spin relaxation [8]. The mechanism is briefly sketched in figure 5(d) where we, as in the inset of figure 3, take into account the spin–orbit splitting of the subbands due to $\sigma_z k_x$-terms in the effective Hamiltonian. The difference in carrier populations in the spin branches $s_z = \pm 1/2$ of the ground subband ($n_\uparrow > n_\downarrow$) causes spin relaxation. The rate of spin-flip scattering depends on the electron wavevectors in the initial and final states that are illustrated by bent arrows of different thicknesses. The transitions of different rates lead to an asymmetric distribution of electrons within each spin branch. As a result an electric current j_x arises. A symmetry analysis shows that the relaxation of the spin component S_y is also accompanied by generation of an electric current along the x-direction.

The process of the third stage, SGE, was already studied in [8, 20, 23]. Therefore, we concentrate below on the first two stages and consider them as a specific kind of optical orientation of electron spins, which is caused by simultaneous transfer of photon linear and angular momenta to the carriers.

The intersubband light absorption in n-doped QW structures is a resonant process and is possible if the photon energy equals the energy spacing between the subbands. In the single-band approximation, direct optical transitions from the subband $e1$ to the subband $e2$ conserve spin orientation and can be induced only under oblique incidence of the light with nonzero p component of polarization. These selection rules are violated if one takes into account $\mathbf{k}\cdot\mathbf{p}$ admixture of the valence-band states to the conduction-band wavefunctions. In this model the light of both s- and p-polarization can induce intersubband optical transitions, and the transitions become spin dependent [21, 22]. We assume that electrons occupy the ground subband $e1$ and the size-quantization energy is substantially larger than the mean kinetic energy in the QW plane. Then, the spin matrix of electron photogeneration in the subband $e1$ has the form

$$G_{\mathbf{k}} = -\frac{2\pi}{\hbar} M^{\dagger} M f_{\mathbf{k}}\, \delta(\hbar\omega + \varepsilon_{1,\mathbf{k}} - \varepsilon_{2,\mathbf{k}+\mathbf{q}_\parallel}), \tag{9}$$

where M is a 2×2 matrix describing the intersubband optical transitions, M is the hermitian conjugate matrix, $f_{\mathbf{k}}$ is the function of equilibrium carrier distribution, $\varepsilon_{1,\mathbf{k}} = \hbar^2 k^2/2m^*$ and $\varepsilon_{2,\mathbf{k}} = \varepsilon_{21} + \hbar^2 k^2/2m^*$ are the electron dispersions in the subbands $e1$ and $e2$, respectively, m^* is the effective electron mass, ε_{21} is the energy spacing between the subbands, and $\mathbf{q}_\parallel$ is the in-plane component of the photon wavevector. The δ-function in (9) reflects the resonant behavior of the intersubband optical transitions. In real QW structures the spectral width of the resonance is broadened due to finite scattering time of carriers, fluctuations of the QW width, etc. To describe the broadening one can replace the δ-function by a normalized function δ_Γ which corresponds to the absorption spectrum in the real structure. To first order in the $\mathbf{k}\cdot\mathbf{p}$ theory, the matrix M is given by [22]

$$M = -\frac{eA}{cm^*}\, p_{21} \begin{bmatrix} e_z & \Lambda(e_x - \mathrm{i}e_y) \\ -\Lambda(e_x + \mathrm{i}e_y) & e_z \end{bmatrix}, \tag{10}$$

where A is the amplitude of the electro-magnetic wave related to the light intensity by $I = A^2\omega^2 n_\omega/(2\pi c)$, c is the light velocity, and p_{21} is the momentum matrix element between

the envelope functions of size quantization $\varphi_1(z)$ and $\varphi_2(z)$ in the subbands $e1$ and $e2$,

$$p_{21} = -\mathrm{i}\hbar \int \varphi_2(z) \frac{\partial}{\partial z} \varphi_1(z)\, \mathrm{d}z. \tag{11}$$

The parameter Λ originates from $\mathbf{k}\cdot\mathbf{p}$ admixture of valence-band states to the electron wavefunction and is given by

$$\Lambda = \frac{\varepsilon_{21}\Delta(2E_\mathrm{g}+\Delta)}{2E_\mathrm{g}(E_\mathrm{g}+\Delta)(3E_\mathrm{g}+2\Delta)}, \tag{12}$$

where E_g is the energy of the band gap, and Δ is the energy of spin–orbit splitting of the valence band.

Absorption of circularly polarized light leads to spin orientation of photoexcited carriers. We assume that the momentum relaxation time τ_{e1} is shorter than the precession period in the effective magnetic field, $\Omega\tau_{e1} \ll 1$. Then, the spin generation rate in the subband $e1$ has the form [24]

$$\dot{\mathbf{S}} = \sum_{\mathbf{k}} \mathbf{g}_\mathbf{k} + \sum_{\mathbf{k}} \tau_{e1}[\Omega \times \mathbf{g}_\mathbf{k}], \tag{13}$$

where $\mathbf{g}_\mathbf{k} = \mathrm{Tr}(\sigma G_\mathbf{k})/2$ is the rate of spin photogeneration into states with the wave vector $\mathbf{k}$, σ is the vector of the Pauli matrices. The first term in (13) describes optical orientation of carriers in the moment of photoexcitation, while the second term stands for spin orientation, which is caused by spin dependent asymmetry of excitation in $\mathbf{k}$-space followed by spin precession in the effective magnetic field. It is the term that describes optical orientation by circularly polarized light, which is related to the transfer of photon linear momenta to charge carriers and vanishes if $\mathbf{q}_\parallel = 0$.

In asymmetrically (110)-grown QW structures the Larmor frequency corresponding to the effective magnetic field has the form

$$\Omega = \frac{2}{\hbar}(\beta_{xy}k_y,\ \beta_{yx}k_x,\ \beta_{zx}k_x), \tag{14}$$

where β_{xy}, β_{yx} and β_{zx} are constants of the spin–orbit interaction. As in the experiment described above, we consider that the light wavevector $\mathbf{q}$ lies in the xz-plane. Then, for the Boltzmann distribution of carriers, one derives

$$\dot{S}_x = \Lambda\eta_z(\hbar\omega)\frac{q_x}{2q}\frac{I P_\mathrm{c}}{\hbar\omega}, \tag{15}$$

$$\dot{S}_y = -q_x\,\bar{\varepsilon}\,\Lambda\frac{\beta_{zx}\tau_{e1}}{\hbar}\frac{q_x}{q}\frac{\mathrm{d}\,\eta_z(\hbar\omega)}{\mathrm{d}\,\hbar\omega}\frac{I P_\mathrm{c}}{\hbar\omega}, \tag{16}$$

$$\dot{S}_z = \left[\eta_z(\hbar\omega)\Lambda^2\frac{q_z}{2q} + q_x\bar{\varepsilon}\,\Lambda\frac{\beta_{yx}\tau_{e1}}{\hbar}\frac{q_x}{q}\frac{\mathrm{d}\,\eta_z(\hbar\omega)}{\mathrm{d}\,\hbar\omega}\right]\frac{I P_\mathrm{c}}{\hbar\omega}, \tag{17}$$

where $\bar{\varepsilon} = k_\mathrm{B}T$ is the mean kinetic energy of equilibrium carriers, T is the temperature, $\eta_z(\hbar\omega)$ is the QW absorbance for light polarized along the growth direction,

$$\eta_z(\hbar\omega) = \frac{4\pi^2\alpha}{n_\omega}\frac{\hbar|p_{21}|^2}{m^{*2}\omega}\, n_s\, \delta_\Gamma(\hbar\omega - \varepsilon_{21})\,, \tag{18}$$

and α is the fine-structure constant.

As addressed above, relaxation of spin components S_y and S_z in (110)-oriented QW structures is accompanied by the generation of an electric current along the x-axis due to the SGE. Equations (16) and (17) show that spin components S_y and S_z contain contributions proportional to the photon wavevector q_x and the light helicity P_c. Therefore, the generated photocurrent can be gathered in a class of photon drag effects denoted as the circular photon drag effect.

5. Conclusion

We demonstrated that in (110)-grown GaAs QWs, circular polarized infrared radiation and THz radiation induce photocurrents which change sign upon reversing the radiation helicity. It is shown that two microscopic mechanisms, comprising the CPGE and the circular photon drag effect, are responsible for these photocurrents. The microscopic mechanism of current formation by the CPGE is closely related to photocurrents observed in (113)-oriented n-type GaAs QWs [21]. To describe the circular photon drag effect we developed a microscopic theory which explains all observed features including helicity and angle of incidence dependencies. The theory is based on optical spin orientation being sensitive to the photon wavevector. Subsequent asymmetric spin relaxation results in the photocurrent.

Acknowledgments

We are grateful to E L Ivchenko for helpful discussions and thank I Gronwald for technical assistance. This work was supported by the Deutsche Forschungsgemeinschaft through SPP 1285, SFB 689 and GRK638, the RFBR, programs of the RAS and the Russian Ministry of Education and Science, Russian Science Support Foundation, and Foundation 'Dynasty'—ICFPM.

References

[1] Ohno Y, Terauchi R, Adachi T, Matsukura F and Ohno H 1999 *Phys. Rev. Lett.* **83** 4196
[2] Karimov O Z, John G H, Harley R T, Lau W H, Flatte M E, Henini M and Airey R 2003 *Phys. Rev. Lett.* **91** 246601
[3] Dohrmann S, Hagele D, Rudolph J, Bichler M, Schuh D and Oestreich M 2004 *Phys. Rev. Lett.* **93** 147405
[4] Hall K C, Gundogdu K, Hicks J L, Kocbay A N, Flatte M E, Boggess T F, Holabird K, Hunter A, Chow D H and Zinck J J 2005 *Appl. Phys. Lett.* **86** 202114
[5] Ganichev S D, Ivchenko E L, Danilov S N, Eroms J, Wegscheider W, Weiss D and Prettl W 2001 *Phys. Rev. Lett.* **86** 4358
[6] Bieler M, Laman N, van Driel H M and Smirl A L 2005 *Appl. Phys. Lett.* **86** 061102
[7] Yang C L, He H T, Ding Lu, Cui L J, Zeng Y P, Wang J N and Ge W K 2006 *Phys. Rev. Lett.* **96** 186605
[8] Ganichev S D, Ivchenko E L, Bel'kov V V, Tarasenko S A, Sollinger M, Weiss D, Wegscheider W and Prettl W 2002 *Nature* **417** 153
[9] Ganichev S D and Prettl W 2006 *Intense Terahertz Excitation of Semiconductors* (Oxford: Oxford University Press)
[10] Ivchenko E L 2005 *Optical Spectroscopy of Semiconductor Nanostructures* (Harrow, UK: Alpha Science International)
[11] Ivchenko E L and Pikus G E 1986 *Semiconductor Physics* ed V M Tuchkevich and V Ya Frenkel (New York: Consultant Bureau) p 427

[12] Belinicher V I 1981 *Fiz. Tverd. Tela* **23** 3461
Belinicher V I 1981 *Sov. Phys. Solid State* **23** 2012 (Engl. Transl.)
[13] Yaroshetskii I D and Ryvkin S M 1986 *Semiconductor Physics* ed V M Tuchkevich and V Ya Frenkel (New York: Consultant Bureau) p 249
[14] Gibson A F and Kimmitt A F 1980 *Infrared and Millimeter Waves*, vol 3: *Detection of Radiation* ed K J Button (New York: Academic) p 181
[15] Luryi S 1987 *Phys. Rev. Lett.* **58** 2263
[16] Wieck A D, Sigg H and Ploog K 1990 *Phys. Rev. Lett.* **64** 463
[17] Shalygin V A *et al* 2006 *JETP Lett.* **84** 570
[18] Magarill L I and Entin M V 1982 *Poverkhnost'* **1** 74 (in Russian)
[19] Gusev G M, Kvon Z D, Magarill L I, Palkin A M, Sozinov V I, Shegai O A and Entin M V 1987 *Pis. Zh. Eksp. Teor. Fiz.* **46** 28
Gusev G M, Kvon Z D, Magarill L I, Palkin A M, Sozinov V I, Shegai O A and Entin M V 1987 *Sov.—JETP Lett.* **46** 33 (Engl. Transl.)
[20] Ganichev S D *et al* 2003 *Phys. Rev.* B **68** 081302
[21] Ganichev S D, Bel'kov V V, Petra S., Ivchenko E L, Tarasenko S A, Wegscheider W, Weiss D, Schuh D, Beregulin E V and Prettl W 2003 *Phys. Rev.* B **68** 035319
[22] Ivchenko E L and Tarasenko S A 2004 *Zh. Eksp. Teor. Fiz.* **126** 426
Ivchenko E L and Tarasenko S A 2004 *JETP* **99** 379 (Engl. Transl.)
[23] Ivchenko E L, Lyanda-Geller Yu B and Pikus G E 1990 *Zh. Eksp. Teor. Fiz.* **98** 989
Ivchenko E L, Lyanda-Geller Yu B and Pikus G E 1990 *Sov. Phys.—JETP* **71** 550 (Engl. Transl.)
[24] Tarasenko S A 2005 *Phys. Rev.* B **72** 113302